THE JOURNAL OF PHYSICAL CHEMISTRY A
A JOURNAL OF THE AMERICAN CHEMICAL SOCIETY

pubs.acs.org/JPCA

Article

Computational Investigation of the Formation of Peroxide (ROOR) Accretion Products in the OH- and NO_3-Initiated Oxidation of α-Pinene

Galib Hasan,* Rashid R. Valiev, Vili-Taneli Salo, and Theo Kurtén*

Cite This: *J. Phys. Chem. A* 2021, 125, 10632−10639

Read Online

ACCESS | Metrics & More | Article Recommendations | Supporting Information

ABSTRACT: The formation of accretion products ("dimers") from recombination reactions of peroxyl radicals (RO_2) is a key step in the gas-phase generation of low-volatility vapors, leading to atmospheric aerosol particles. We have recently demonstrated that this recombination reaction very likely proceeds via an intermediate complex of two alkoxy radicals (RO···OR′) and that the accretion product pathway involves an intersystem crossing (ISC) of this complex from the triplet to the singlet surface. However, ISC rates have hitherto not been computed for large and chemically complex RO···OR′ systems actually relevant to atmospheric aerosol formation. Here, we carry out systematic conformational sampling and ISC rate calculations on ^{3}(RO···OR′) clusters formed in the recombination reactions of different diastereomers of the first-generation peroxyl radicals originating in both OH- and NO_3-initiated reactions of α-pinene, a key biogenic hydrocarbon for atmospheric aerosol formation. While we find large differences between the ISC rates of different diastereomer pairs, all systems have ISC rates of at least 10^6 s^{-1}, and many have rates exceeding 10^{10} s^{-1}. Especially the latter value demonstrates that accretion product formation via the suggested pathway is a competitive process also for α-pinene-derived RO_2 and likely explains the experimentally observed gas-phase formation of C_{20} compounds in α-pinene oxidation.

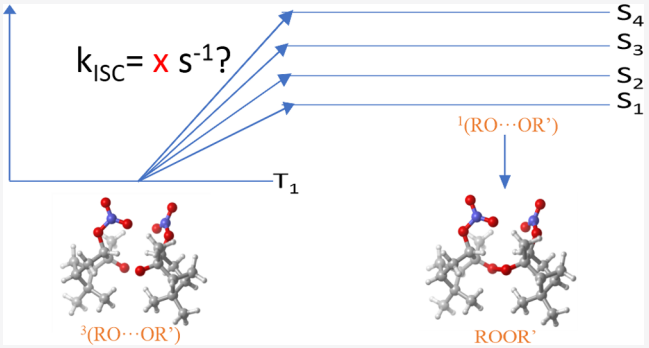

INTRODUCTION

Organic peroxyl radicals (RO_2•) are important molecules in the atmosphere because their reactions play a significant role in the formation of low-volatility products, leading to secondary organic aerosol (SOA) particles. Atmospheric aerosols, especially fine <1 μm and ultrafine <100 nm particles, are regarded as one of the key species responsible for air pollution-related mortality.[1] They also affect the climate by cloud, mist, and fog formation[2] and contribute to the earth's energy budget by scattering and absorbing solar radiation and by forming cloud condensation nuclei.[3] Aerosol-related effects are regarded as one of the least understood components of global radiative forcing.[4]

SOA formation is driven by the oxidation of volatile organic compounds (VOC) such as anthropogenic or biogenic hydrocarbons.[5] As the direct addition of O_2 to hydrocarbons is spin-forbidden (at least for ground-state singlet products), this oxidation is initiated by a small number of photochemically generated oxidants: OH, O_3, Cl, and NO_3.[6,7] The details of the oxidation mechanisms depend on the hydrocarbon-oxidant combination, but inevitably involve the formation of peroxyl radicals (RO_2). In most atmospheric conditions, the main sink of RO_2 is the reaction with either nitric oxide (NO) or with the hydroperoxyl radical (HO_2). Self- and cross-reactions of RO_2 can be major side channels and are especially important for aerosol formation because of their potential to form "dimers": low-volatility accretion products retaining most or all of the carbon atoms of the original hydrocarbons.

The molecular-level mechanism of RO_2 + $R'O_2$ reactions was identified as a major open question in atmospheric science already in 2009.[8] Using multireference quantum chemical calculations,[9,10] we have recently confirmed the feasibility of the reaction mechanism postulated by Ghigo et al.[11] and Lee et al.[12] (see Scheme 1 for illustration). Briefly, all reaction pathways start on an overall singlet potential energy surface and involve at least two intermediates: RO_4R' tetroxides as postulated already by the Russell mechanism in 1959[13] and RO···O_2···R′O complexes. For the reaction to be thermodynamically feasible, O_2 must be formed in its triplet ground state. This, in turn, requires that the two alkoxy radicals (RO and R′O) are also coupled as a triplet, preventing immediate

Received: October 14, 2021
Revised: November 29, 2021
Published: December 9, 2021

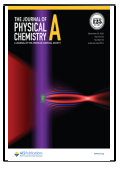

https://doi.org/10.1021/acs.jpca.1c08969
J. Phys. Chem. A 2021, 125, 10632−10639

Scheme 1. Mechanism for the Cross-Reaction between Two Peroxyl Radicals (RO_2), and Possible End Products

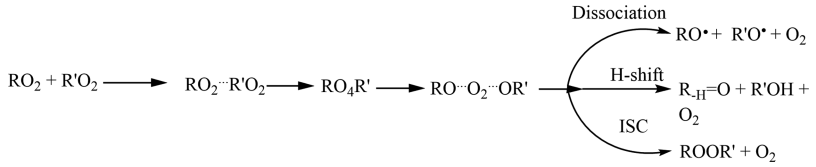

Scheme 2. Major Reaction Pathways for the α-pinene + NO_3 and α-pinene + OH Systems

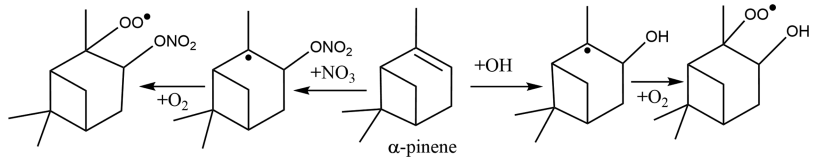

recombination because of the Pauli principle. The different reaction channels available to a given RO_2 + R′O_2 combination then correspond to different fates of ^{3}(RO···OR′) complexes, which are left after the (presumably very weakly bound) $^3O_2$ has dissociated from the RO···O_2···R′O system. For example, the dissociation of the cluster leads to RO + R′O products, and intermolecular hydrogen shifts lead to alcohol and carbonyl products. A third possibility is an intersystem crossing (ISC) to the singlet potential energy surface, and subsequent recombination of the alkoxy radicals to form peroxide (ROOR′) products. Our calculations on a variety of relatively simple model systems[9] demonstrate that all of these channels may have high rate constants, on the order of 10^9 s^{-1} or more. This suggests that the experimentally observed gas-phase formation of accretion products in various hydrocarbon oxidation systems[14] may indeed proceed through the ISC of ^{3}(RO···OR′) complexes. However, ISC rates have so far not been systematically computed for actual SOA-relevant systems such as monoterpene oxidation products.

Monoterpenes, with elemental composition $C_{10}H_{16}$, are biogenic hydrocarbons believed to be important especially for the first steps of SOA formation. The reason for this is that they are large and complex enough to form oxidation products with very low volatilities, while still having high enough emission rates and atmospheric concentrations. α-pinene is one of the most important monoterpenes, accounting for approximately half of all monoterpene emissions.[15] Reactions between α-pinene and atmospheric oxidants produce a range of products, including multifunctional low-volatility accretion products with up to 20 carbon atoms.[16] We studied RO_2 formed in the OH- and NO_3-initiated oxidation of α-pinene because their structures are unambiguously known and because they have relatively few conformers (compared, for example, to O_3-derived RO_2). Scheme 2 depicts the major reaction routes for the oxidation of α-pinene by OH and NO_3. Basically, the major route involves the addition of OH or NO_3 to the less highly substituted olefinic carbon atom[7,17] (H abstraction and/or addition to the other olefinic carbon are possible, but minor, channels). In both cases, the product is an alkylfree radical. O_2 rapidly adds to this free radical and forms a peroxyl radical RO_2.[18]

While atmospheric chemistry studies of monoterpenes have traditionally focused mainly on O_3- and OH-initiated oxidation, recent global modeling studies of organic aerosol[19−21] suggest that a large fraction of SOA[22,23] is produced from the oxidation of biogenic organic compounds by the nitrate radical (NO_3), possibly more than that produced by OH oxidation. Recent studies have further shown that NO_3 oxidation is not only a night-time process, but happens also during the day.[24,25] In addition, field analysis of organonitrate diurnal variations demonstrates that NO_3 oxidation chemistry makes significant contribution to the production of organonitrates.[26−28] Depending on their subsequent photochemistry, organo-nitrates formed by NO_3-initiated oxidation constitute a large NO_x reservoir.[29]

In this study, we systematically compute energetics for a large set of ^{3}(RO···OR′) clusters corresponding to the relevant RO_2 + R′O_2 systems. We consider different stereoisomers of RO derived from the major RO_2 formed in the OH- and NO_3-initiated oxidation α-pinene (shown in the right and left sides of Scheme 2, respectively). Because of the presence of two stereocenters, there are four stereoisomers in each system. We denote these as α-pinene, (1) S-alkoxy, R-hydroxy/nitroxy, (2) R-alkoxy, S-hydroxy/nitroxy, (3) S-alkoxy, S-hydroxy/nitroxy, and (4) R-alkoxy, R-hydroxy/nitroxy. In our previous work, we developed a configurational sampling approach for ^{3}(RO···OR′) clusters.[30] We use the same approach here to search for the global minimum-energy conformer for each cluster type, considering the homodimers [i.e., ^{3}(RO···OR′) clusters, where RO and RO′ are the same species] of all monomer stereoisomers. Dimers consisting of different monomer stereoisomers were not considered because of computational reasons (i.e., the large number of such systems). We are not aware of any reported stereoselectivity of the reactions shown in Scheme 2 (or of any of the competing RO_2 sink reactions), and thus, the collision of each combination of two stereoisomers could be presumed equally likely. The set of ^{3}(RO···OR′) clusters studied here should thus be considered a representative subset. However, as discussed below, our results on the alkoxy-nitroxy systems tentatively suggest that the formation of one of the four stereoisomers may be energetically unfavorable compared to the others.

For the studied ^{3}(RO···OR′) clusters, we then calculated the ISC rate constant using state-of-the-art multireference methods. We did not study the H-shift channel in this work because there are no H atoms to abstract on the tertiary α-oxyl carbon. The conventional "alcohol + carbonyl" channel is thus not possible for the studied RO_2/RO systems. Hypothetical H-shifts from other C atoms are likely to have high barriers because of a combination of steric strain and the formation of diradical products.

We note that while the overall self-reaction rate of tertiary peroxy radicals is often low, OH-substituted tertiary peroxy radicals can have self-reaction rate coefficients on the order of

https://doi.org/10.1021/acs.jpca.1c08969
J. Phys. Chem. A 2021, 125, 10632−10639

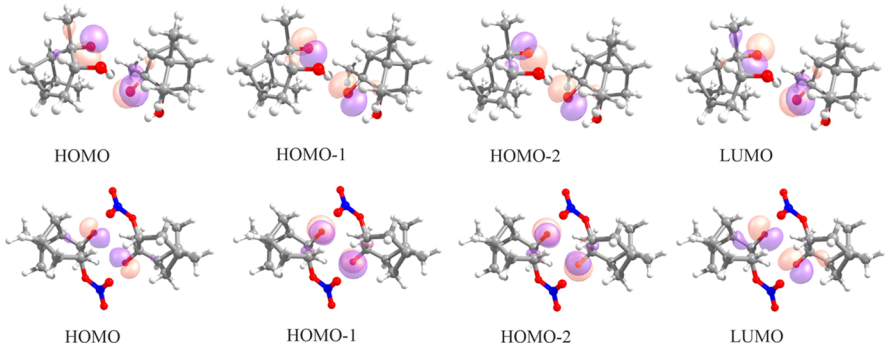

Figure 1. Orbitals included in the (6,4) active space for α-pinene, (*S*-alkoxy,*R*-hydroxy)$_2$ and α-pinene, (*R*-alkoxy,*R*-nitroxy)$_2$. HOMO and LUMO refer to the highest occupied and lowest unoccupied molecular orbitals, respectively. Color coding: gray = C, red = O, white = H, and blue = N.

10^{-14} cm^3 mol^{-1} s^{-1}.[7] If accretion product (ROOR′) formation is the dominant channel for these reactions, they may be atmospherically relevant despite representing a relatively minor RO_2 sink compared to reactions with NO or HO_2.

THEORY AND METHODS

Conformational Sampling of the Alkoxy Radical Monomers. The systematic conformer search algorithm in Spartan version 16 was used for generating all the conformers of the alkoxy monomers (RO•).[31] In this approach, every nonterminal bond is rotated by 180 degrees for sp^2-hybridized atoms and 120 degrees for sp^3-hybridized atoms. Possible ring flipping was also considered during this conformer searching. A molecular mechanics force-field (MMFF) optimization was then performed to find representative sets of all the local minima conformers on the potential energy surfaces (PES). We found a maximum of three conformers for each alkoxy radical stereoisomer because torsional rotations are limited by the intact bicyclic α-pinene skeleton (see Scheme 2). We used the keyword ("ffhint = O_x ~ ~6," denoting generic divalent O) to avoid the treatment of alkoxy radical oxygens as anions.[32] (We note that this issue has been resolved in newer versions of Spartan, from 18 onward). For the S-alkoxy,*R*-nitroxy system, conformational sampling with Spartan 16 yielded only one monomer conformer. This structure was therefore resampled using Spartan 20, leading to three conformers, which were then used in the subsequent sampling of ^{3}(RO···OR′) clusters.

Systematic Conformational Sampling of ^{3}(RO···OR′) Clusters. The conformational sampling of ^{3}(RO···OR′) clusters involved several steps. First, thousands of initial conformers were generated using the artificial bee colony (ABC) algorithm, which performs rigid-body molecular dynamics.[33,34] The ABC algorithm requires monomer structures, as well as Lennard-Jones parameters and partial charges for all atoms in the monomers. Structures and partial charges were obtained from optimizations and natural bonding orbital (NBO) calculations at the ωB97X-D/6-31++G** level of theory using Gaussian16 RevB.01.[35] The Lennard-Jones parameters were collected from the CHARMM force-field database. We initially generated 3000 cluster conformers for every combination of monomer conformers. As described above, each monomer had a maximum of three conformers, leading to six distinct combinations of two monomer conformers. Thus, a total of up to 18,000 conformers were generated for each of the eight studied stereoisomers. Semiempirical optimization was then carried out using the XTB program and the GFN-*x*TB (Geometry, Frequency, Noncovalent, eXtended Tight Binding) level of theory[36] for all the conformers generated using the ABC algorithm. At this stage, various unwanted reactions, typically combinations of H-shifts and C−C bond scissions, took place because of a combination of strained input geometries and (likely artificially) low reaction barriers at the GFN-*x*TB level. Section S1 of the Supporting Information shows some examples of unwanted reactions at the XTB level. We tested different keyword settings in the XTB program to get rid of this problem. We found that performing the semiempirical optimizations with loose optimization criteria helped get rid of most of the unwanted reactions at least for the clusters studied here. Conformers within 10 kcal/mol of the lowest-energy structure for each system were then selected for density functional level (DFT) calculations. Because of the large size of the α-pinene systems, computational costs prevented us from carrying out calculations at the same level as in our previous studies (coupled cluster singles, doubles and perturbative triples [CCSD(T)] energies on ωB97X-D/aug-cc-pVTZ structures). Therefore, DFT optimizations were performed at the ωB97X-D/6-31++G** level of theory[37,38] using Gaussian16 RevB.01.[39] Electronic energies and dipole moments were then collected from all conformers, and duplicate structures (with identical energies and dipole moments) were eliminated. Finally, ωB97X-D/6-31++G** frequency calculations were performed on conformers within 5 kcal/mol of the lowest-energy structure for each system. We note that while binding energetics computed at this level should be considered qualitative, the actual cluster geometries used for the ISC rate calculations are likely much less sensitive to the size of the basis set. The ISC rates presented here should thus be comparable to our previous studies.

ISC RATE CALCULATION

^{3}(RO···OR′) clusters can undergo ISC to the singlet surface, allowing for (presumably near-instantaneous) recombination to covalently bound ROOR accretion products. The details of our ISC rate calculations are explained in our previous work.[9,10] In brief, the global minimum conformers from the DFT calculations described above, as well as one other conformer per system (the lowest-energy conformer that had a clearly different bonding pattern compared to the global minimum), were selected, and the energies of the lowest four singlet and triplet states were computed at the XMC-QDPT2/6-311++G** level of theory using Firefly, version 8.2.0.[40] The ISC rate coefficient, k_{ISC} (in units of s^{-1}), was then obtained using the following formula:

https://doi.org/10.1021/acs.jpca.1c08969
J. Phys. Chem. A 2021, 125, 10632−10639

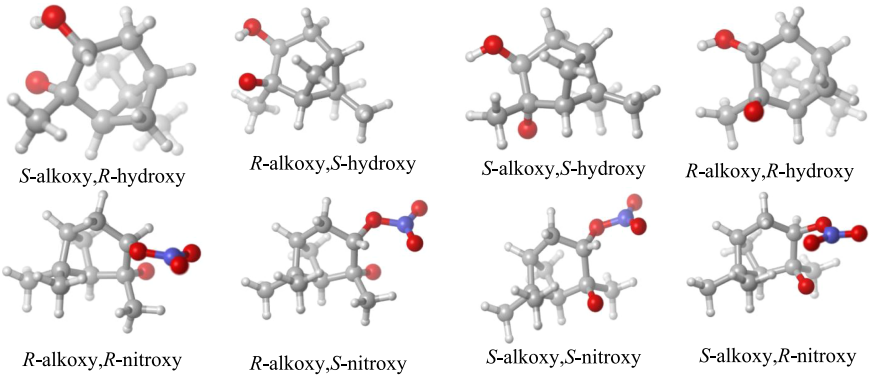

Figure 2. Optimized lowest-energy structures at the ωB97X-D/6-31++G** level of theory of different stereoisomers of the hydroxy-alkoxy and nitroxy-alkoxy radicals formed in the oxidation of α-pinene by OH and NO_3, assuming initial radical addition to the secondary carbon atom (as depicted in Scheme 2, followed by the loss of one oxygen from the peroxy radicals to form alkoxy radicals). Color coding: gray = C, white = H, red = O, and blue = N.

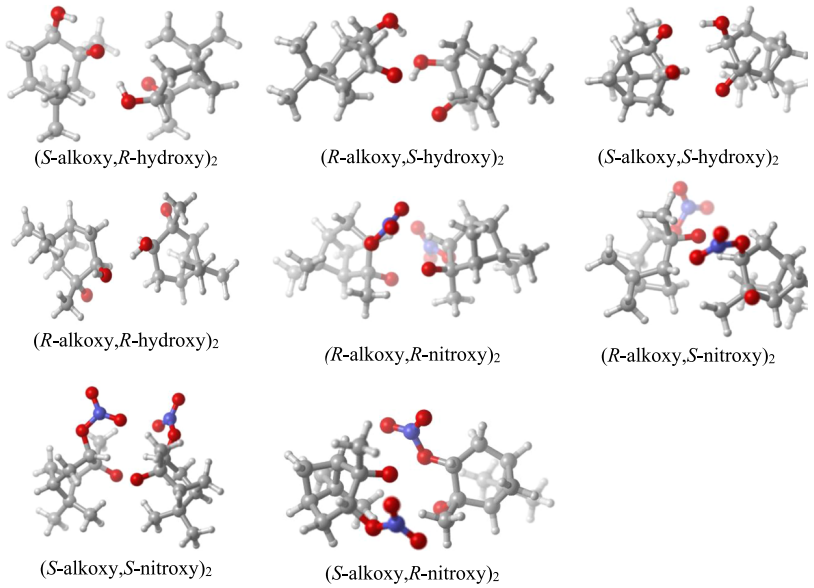

Figure 3. Optimized lowest-energy structures of the ^{3}(RO···OR′) clusters studied in this work at the ωB97X-D/6-31++G** level of theory. Color coding: gray = C, white = H, red = O, and blue = N.

$$k_{ISC}(T_i \rightarrow S_j) = 1.6 \times 10^9 \cdot \langle \varphi(T_i) | \hat{H}_{SO} | \varphi(S_j) \rangle^2 \cdot F_{ij} \quad (1)$$

where $\langle \varphi(T_i) \mid \hat{H}_{SO} \mid \varphi(S_j) \rangle$ is the spin-orbit coupling matrix element (SOCME) in cm^{-1}, and F_{ij} is Franck−Condon's factor (which depends on the energy gap between the states). We tested several different active spaces to check which sets of orbitals contribute to the state averaging. We found that the (6,4) active space (six electrons in four orbitals) represents a good compromise between the computational cost and accuracy and is sufficient to describe the states of interest. The details of the active space selection followed the philosophy described in our previous work.[10] The selected molecular orbitals, mainly formed from *p*-atomic orbitals of the radical oxygen atoms, are those that give the largest contributions (configuration interaction weights of more than 0.2) to the relevant low-lying electronic states (T_1...T_4 and S_1...S_4). Figure 1 shows the orbitals included in the active space for two of the eight studied systems (one alkoxy-hydroxy and one alkoxy-nitroxy radical pair). The orbitals for other stereoisomer pairs look similar. ISC rates were computed for transitions from the triplet ground state T_1 to the four lowest singlet states (S_1...S_4).

The matrix element of the spin-orbit coupling interaction between triplet T_1-T_4 and singlet states S_1-S_4 was calculated at the CASSCF(6,4)/ 6-311++G** level of theory, but using the XMC-QDPT2/6-311++G** energies, with the general atomic and molecular electronic structure system (GAMESS-US) program.[41]

RESULTS AND DISCUSSION

Minimum-energy conformers of the RO monomers are shown in Figure 2, while the minimum-energy conformers of the ^{3}(RO···OR′) clusters are given in Figure 3. (Structures and relative energies of local minima are given in Section S4 of the Supporting Information). The relative binding energies of the ^{3}(RO···OR′) clusters (expressed in terms of the energies and Gibbs free energies of the ^{3}(RO···OR′) → RO + R′O reaction) are given in Table 1. Consistent with the DFT results on smaller functionalized RO in our previous study,[9] the electronic energies of the dissociation reaction mostly vary between about 9 and 12 kcal/mol, while the corresponding

https://doi.org/10.1021/acs.jpca.1c08969
J. Phys. Chem. A 2021, 125, 10632−10639

Table 1. Electronic Energies (in kcal/mol) and Gibbs Free Energies (in kcal/mol at 298 K and 1 atm Reference Pressure) for the ^{3}(RO···OR′) → RO + R′O Reaction Computed at ωB97X-D/6-31++G Level of Theory**

^{3}(RO···OR′) cluster	ΔE in kcal/mol	ΔG in kcal/mol	O···O radical distance in Å
α-pinene, (*S*-alkoxy,*R*-hydroxy)$_2$	+9.14	−3.12	3.31
α-pinene, (*R*-alkoxy,*S*-hydroxy)$_2$	+9.10	−2.96	3.35
α-pinene, (*S*-alkoxy,*S*-hydroxy)$_2$	+9.76	−2.22	4.13
α-pinene, (*R*-alkoxy,*R*-hydroxy)$_2$	+11.96	+0.97	3.50
α-pinene, (*R*-alkoxy,*R*-nitroxy)$_2$	+10.71	−1.89	3.19
α-pinene, (*R*-alkoxy,*S*-nitroxy)$_2$	+10.18	−1.63	5.49
α-pinene, (*S*-alkoxy,*S*-nitroxy)$_2$	+10.83	−2.61	3.48
α-pinene, (*S*-alkoxy,*R*-nitroxy)$_2$	+18.19	+6.34	4.32

Gibbs free energies vary between about 1 and −3 kcal/mol. These values are typical for fairly weakly bonded clusters in the atmosphere. The α-pinene,(*S*-alkoxy,*R*-nitroxy)$_2$ cluster is an outlier, with considerably stronger bonding than any of the other clusters. As seen from Figure 3, this cluster has a direct interaction between the alkoxy radical on one monomer and the nitroxy group of the other monomer. Most other alkoxy-nitroxy clusters in this study, as well as the simpler alkoxy-nitroxy clusters in our previous study,[9] had global minimum structures (at the at ωB97X-D level) characterized by nitroxy-nitroxy interactions. The α-pinene,(*R*-alkoxy,*S*-nitroxy)$_2$ cluster also contains an alkoxy-nitroxy interaction, but has a much lower binding energy. Upon closer inspection, the anomalous binding energy of the α-pinene,(*S*-alkoxy,*R*-nitroxy)$_2$ system is driven mainly by differences in monomer energies: the α-pinene, *S*-alkoxy,*R*-nitroxy radical monomer is between 1.6 and 4.0 kcal/mol higher in absolute energy than the other three alkoxy-nitroxy radicals, presumably because of less favorable interactions between the nitroxy group and the rest of the molecule in the monomer. As the monomer energy is multiplied by two in the binding energy calculation, this alone leads to a difference between 3.2 and 8.0 kcal/mol in the binding energies in favor of the α-pinene, (*S*-alkoxy,*R*-nitroxy)$_2$ system. In contrast, the differences in absolute energies of the four different alkoxy-nitroxy clusters shown in Figure 3 are less than 5 kcal/mol. To ensure that the presented α-pinene, (*S*-alkoxy,*R*-nitroxy)$_2$ structure is not a computational artifact, we have recomputed its binding energy with the same basis set, but using four different functionals (PW6B95D3, M05-2X, M06-2X, and LC-wPBE, using GD3 empirical dispersion), and found similar results, as obtained at the ωB97X-D/6-31++G** level. We also manually constructed clusters with similar bonding patterns for the other three systems in order to rule out the possibility that the "anomalous" bonding pattern is actually the correct one but was simply missed for the other three cases because of the limitations of our conformational sampling algorithm. However, these did not lead to lower-energy clusters than those already discovered in the sampling. Based on these test calculations, we tentatively conclude that the anomalously strong binding of the α-pinene, (*S*-alkoxy,*R*-nitroxy)$_2$ system represents an example of genuinely strong stereoselectivity in cluster formation. However, we note that the high (unfavorable) energy of the corresponding monomer, assuming a similar pattern, also found for the parent peroxy-nitroxy radicals, may also cause stereoselectivity in the formation reaction: the *S*-peroxy,*R*-nitroxy stereoisomer may have a much lower yield than the others.

Even if the *S*-alkoxy,*R*-nitroxy system is excluded, the nitroxy-alkoxy radical dimers are generally somewhat more strongly bound than their hydroxy-alkoxy counterparts, which is surprising as the latter have H-bonds while the former do not. This is likely explained by the presence of intramolecular H-bonds in the hydroxy-alkoxy radical monomers. These act to decrease the energies (and free energies) of the monomers, leading to relatively weaker binding of the clusters. The distance between the two radical oxygen atoms did not correlate significantly with the cluster binding energy, likely because even the shortest distances were above 3 Å (implying little interaction).

The overall ISC rate constants for our studied systems (corresponding to a sum of the four-individual computed ISC rates) are given in Table 2. (Data for local minima are given in Section S2 of the Supporting Information.) In our previous work comparing a series of relatively simple functionalized RO,[9,10] we observed that the ISC rates strongly depended on the conformation of the ^{3}(RO···OR′) clusters and displayed extreme stereoselectivity for the two systems included in the study that possessed stereocenters: *R,S*-BuOH-O···O-BuOH and *R,S*-PrNO$_3$-O···O-PrNO$_3$. The present systems also display substantial stereoselectivity: the ISC rates for the global minimum conformers of different stereoisomer pairs of hydroxy-alkoxy and nitroxy-alkoxy triplet clusters vary by almost three and over four orders of magnitude, respectively. The variation between different conformers of the same system is also large, up to four orders of magnitude for the studied pairs of global and local minima. Notably, for some of the systems where the global minimum conformer had a relatively low ISC rate, the local minimum conformer (with a different binding pattern) had a substantially higher rate or vice versa. All computed ISC rates are in any case fairly fast, exceeding 10^7 s^{-1} for all but three of the 16 cases (when including the local minima) and 10^8 s^{-1} for over half the cases.

Table 2. ISC Rate Constants for The Studied Systems at 298 K, Based on Energies of Triplet and Singlet States Computed Using XMC-QDPT2(10,8)/6-311++G and Matrix Elements of the Spin-Orbit Coupling Interaction between T_1-T_4 and S_1-S_4 States Computed at the CASSCF(6,4)/6-31++G** Level**

^{3}(RO···OR′) cluster	Σk_{ISC} (s^{-1})
α-pinene, (*S*-alkoxy,*R*-hydroxy)$_2$	1.18×10^{10}
α-pinene, (*R*-alkoxy,*S*-hydroxy)$_2$	5.68×10^{7}
α-pinene, (*S*-alkoxy,*S*-hydroxy)$_2$	9.43×10^{9}
α-pinene, (*R*-alkoxy,*R*-hydroxy)$_2$	1.51×10^{10}
α-pinene, (*R*-alkoxy,*R*-nitroxy)$_2$	1.62×10^{10}
α-pinene, (*R*-alkoxy,*S*-nitroxy)$_2$	1.02×10^{6}
α-pinene, (*S*-alkoxy,*S*-nitroxy)$_2$	5.68×10^{10}
α-pinene, (*S*-alkoxy,*R*-nitroxy)$_2$	2.06×10^{8}

Section S2 of the Supporting Information shows the relative energies of all considered electronic states, as well as the SOCME values, and the ISC rates for individual transitions. The overall ISC rate of the global minimum conformers is dominated by the ISC between T_1 and S_1 for all the studied

https://doi.org/10.1021/acs.jpca.1c08969
J. Phys. Chem. A 2021, 125, 10632−10639

systems except for two: (*R*-alkoxy,*S*-nitroxy)$_2$ and (*S*-alkoxy,*S*-nitroxy)$_2$. In the former case, the SOCME between T_1 and S_1 is zero, presumably due to the very large distance (5.49 Å) between the radical centers,[42] leading to a zero ISC rate between these states and a low overall ISC rate. In the latter case, the SOCME between the T_1 and S_1 states is small (0.17 cm^{-1}), leading to a modest ISC rate for this transition (4.62×10^7 s^{-1}) despite the fact that the energy gap is negative (i.e., the S_1 state is lower than T_1 for this system, unlike the other seven). However, the overall ISC rate for this system is still high because of the exceptionally high ISC rates between T_1 and S_2 as well as S_3.

The variation in the ISC rate between T_1 and S_1, which determines the overall ISC rate for the remaining six systems, is driven almost exclusively by the variations in the SOCME, as the corresponding energy gaps are very low (less than 80 cm^{-1}). The low energy gap between T_1 and S_1 is consistent with the large distance between the radical centers (Table 2) and the consequent lack of strong interactions between them. The variations in the SOCME between T_1 and S_1 can in turn be related to the orientation of the C−O bonds relative to each other. The wavefunctions of the T_1 and S_1 states have almost the same electronic configuration, with contributions mainly from the 2p atomic orbitals (AO).[42] Thus, the SOCME depends on the overlap between 2p-AOs, belonging to the radical oxygen atoms of two radicals, which in turn depends on their relative orientation.[42,43] In the future, for example, machine-learning approaches could be used to cost-effectively predict SOCME and thus ISC rates for ^{3}(RO···OR′) systems based on the relative orientation of the alkoxy groups.

We further tested the validity of our hypothesis that an ISC in the ^{3}(RO···OR′) clusters will inevitably lead to prompt ^{1}ROOR′ formation. This was done by simply reoptimizing the obtained ^{3}(RO···OR′) minimum-energy structures (shown in Figure 3) on the singlet potential energy surface using the same DFT method (ωB97X-D/6-31++G**). The results of the singlet optimization are shown in Section S3 of the Supporting Information. For five of our eight systems, the optimization yielded the expected formation of ^{1}ROOR′ structures. For the remaining three cases, all of which corresponded to clusters in which the radical centers were relatively far from each other, various other reactions occurred instead, including intramolecular H-shifts and C−C scissions. We caution that while both C−C scissions and H-shifts are well-documented reaction classes of alkoxy radicals, such reactions tend to have at least moderate energy barriers and would not be expected to occur in simple optimizations (energy minimizations). These reactions may thus be artifacts of the relatively low-level optimization method, which is unable to properly treat the ^{1}(RO···OR′) starting point as an open-shell singlet. In any case, these test calculations suggest that ^{1}ROOR′ formation is indeed likely to be the major, although not necessarily the exclusive, end result of an ISC in our ^{3}(RO···OR′) systems.

CONCLUSIONS

Self- and cross-reactions of peroxyl radicals play important roles in both atmospheric and combustion chemistry. For simple peroxyl radicals in the gas phase, the main channels of these reactions correspond to the formation of either two alkoxy radicals or carbonyl and alcohol products. For more complex reactants, experimental studies indicate that also the formation of ROOR′ accretion products is a competitive pathway. Gas-phase accretion product formation provides an efficient mechanism for atmospheric aerosol formation, as it dramatically lowers the volatility of the participating compounds in a single step. Computational studies by us and others suggest that ROOR′ formation is preceded by ISC in weakly bound ^{3}(RO···OR′) complexes formed as an intermediate step in all peroxyl radical self- and cross-reactions. However, actual ISC rates have never been computed for large ^{3}(RO···OR′) systems corresponding, for example, to monoterpene oxidation products. In this study, we first determined the structures and binding energies of ^{3}(RO···OR′) complexes formed in the self-reactions of a set of RO_2 stereoisomers produced in the OH- and NO_3-initiated oxidation of α-pinene. The overall binding energies were fairly weak (around 10 kcal/mol in electronic energy for all but one system) despite the presence of H-bonds in the OH-oxidized systems, implying rapid dissociation rates for the ^{3}(RO···OR′) complexes. The computed ISC rates were also high, exceeding 10^6 s^{-1} for all systems and 10^{10} s^{-1} for some systems. At least the fastest rates should be competitive in atmospheric conditions, confirming the hypothesis that the proposed mechanism can explain accretion product formation observed in α-pinene oxidation experiments. The significant variation of the calculated ISC rates between stereoisomers further implies that accretion product formation might be stereoselective: only some of the RO_2 diastereomers formed in monoterpene oxidation may be able to form ROOR′ effectively. However, the large variation in ISC rates between low-energy conformers of the same stereoisomers is likely to decrease the stereoselectivity of ROOR′ formation.

ASSOCIATED CONTENT

Supporting Information

The Supporting Information is available free of charge at https://pubs.acs.org/doi/10.1021/acs.jpca.1c08969.

Data on local minimum conformers, unwanted reactions occurring in the conformational sampling, results of optimizations on the singlet surface, and detailed ISC rate data for all the systems studied here (PDF)

Quantum chemical output files (ZIP)

AUTHOR INFORMATION

Corresponding Authors

Galib Hasan − *Department of Chemistry, University of Helsinki, Helsinki FIN-00014, Finland; Institute for Atmospheric and Earth System Research, Faculty of Science, University of Helsinki, Helsinki 00014, Finland*; Email: galib.hasan@helsinki.fi

Theo Kurtén − *Department of Chemistry, University of Helsinki, Helsinki FIN-00014, Finland; Institute for Atmospheric and Earth System Research, Faculty of Science, University of Helsinki, Helsinki 00014, Finland*; orcid.org/0000-0002-6416-4931; Email: theo.kurten@helsinki.fi

Authors

Rashid R. Valiev − *Department of Chemistry, University of Helsinki, Helsinki FIN-00014, Finland; Institute for Atmospheric and Earth System Research, Faculty of Science, University of Helsinki, Helsinki 00014, Finland; Research School of Chemistry & Applied Biomedical Sciences, National*

Research Tomsk Polytechnic University, Tomsk 634050, Russia

Vili-Taneli Salo − *Department of Chemistry, University of Helsinki, Helsinki FIN-00014, Finland; Institute for Atmospheric and Earth System Research, Faculty of Science, University of Helsinki, Helsinki 00014, Finland*

Complete contact information is available at: https://pubs.acs.org/10.1021/acs.jpca.1c08969

Notes

The authors declare no competing financial interest.

■ ACKNOWLEDGMENTS

The work was supported by the Academy of Finland, the Jane and Aatos Erkko Foundation (JAES), and the doctoral school of Chemistry and Molecular Science. We thank the Finnish IT Center for Science (CSC) for computational resources. R.R.V. thanks the Ministry of Education and Science of the Russian Federation Program No. 075-03-2021-287/6.

■ REFERENCES

(1) Hallquist, M.; Wenger, J. C.; Baltensperger, U.; Rudich, Y.; Simpson, D.; Claeys, M.; Dommen, J.; Donahue, N. M.; George, C.; Goldstein, A. H.; et al. The formation, properties and impact of secondary organic aerosol: current and emerging issues. *Atmos. Chem.Phys.* **2009**, *9*, 5155−5236.

(2) Daniel, R.; Rosenfeld, D.; Andreae, M. O.; Asmi, A.; Chin, M.; Leeuw, G.; Donovan, D. P.; Kahn, R.; Kinne, S.; Kivekäs, N.; Kulmala, M.; Lau, W.; Sebastian Schmidt, K.; Suni, T.; Wagner, T.; Wild, M.; Quaas, J. Global Observations of Aerosol-Cloud-Precipitation-Climate Interactions. *Rev. Geophys.* **2014**, *52*, 750−808.

(3) Loeb, N. G.; Kato, S. Top-of-Atmosphere Direct Radiative Effect of Aerosols over the Tropical Oceans from the Clouds and the Earth's Radiant Energy System (CERES) Satellite Instrument. *J. Clim.* **2002**, *15*, 1474−1484.

(4) Seinfeld, J. H.; Bretherton, C.; Carslaw, K. S.; Coe, H.; DeMott, P. J.; Dunlea, E. J.; Feingold, G.; Ghan, S.; Guenther, A. B.; Kahn, R.; et al. Improving Our Fundamental Understanding of the Role of Aerosol-Cloud Interactions in the Climate System. *Proc. Natl. Acad. Sci. U. S. A.* **2016**, *113*, 5781−5790.

(5) Jimenez, J. L.; Canagaratna, M. R.; Donahue, N. M.; Prevot, A. S. H.; Zhang, Q.; Kroll, J. H.; DeCarlo, P. F.; Allan, J. D.; Coe, H.; Ng, N. L.; et al. Evolution of Organic Aerosols in the Atmosphere. *Science* **2009**, *326*, 1525−1529.

(6) Glowacki, D. R.; Pilling, M. J. Unimolecular Reactions of Peroxy Radicals in Atmospheric Chemistry and Combustion. *ChemPhysChem* **2010**, *11*, 3836−3843.

(7) Orlando, J. J.; Tyndall, G. S. Laboratory Studies of Organic Peroxy Radical Chemistry: An Overview with Emphasis on Recent Issues of Atmospheric Significance. *Chem. Soc. Rev.* **2012**, *41*, 6294−6317.

(8) Dibble, T. S. Reactions of the Alkoxy Radicals Formed Following OH-Addition to α-Pinene and β-Pinene. C−C Bond Scission Reactions. *J. Am. Chem. Soc.* **2001**, *123*, 4228−4234.

(9) Hasan, G.; Salo, V. T.; Valiev, R. R.; Kubečka, J.; Kurtén, T. Comparing Reaction Routes for ^{3}(RO···OR′) Intermediates Formed in Peroxy Radical Self- and Cross-Reactions. *J. Phys. Chem. A* **2020**, *124*, 8305−8320.

(10) Valiev, R. R.; Hasan, G.; Salo, V.-T.; Kubečka, J.; Kurten, T. Intersystem Crossings Drive Atmospheric Gas-Phase Dimer Formation. *J. Phys. Chem. A* **2019**, *123*, 6596−6604.

(11) Ghigo, G.; Maranzana, A.; Tonachini, G. Combustion and Atmospheric Oxidation of Hydrocarbons: Theoretical Study of the Methyl Peroxyl Self-Reaction. *J. Chem. Phys.* **2003**, *118*, 10575−10583.

(12) Lee, R.; Gryn'ova, G.; Ingold, K. U.; Coote, M. L. Why Are: Sec-Alkylperoxyl Bimolecular Self-Reactions Orders of Magnitude Faster than the Analogous Reactions of Tert-Alkylperoxyls? The Unanticipated Role of CH Hydrogen Bond Donation. *Phys. Chem. Chem. Phys.* **2016**, *18*, 23673−23679.

(13) Russell, G. A. Deuterium-Isotope Effects in the Autoxidation of Aralkyl Hydrocarbons. Mechanism of the Interaction of Peroxy Radicals. *J. Am. Chem. Soc.* **1957**, *79*, 3871−3877.

(14) Bianchi, F.; Tröstl, J.; Junninen, H.; Frege, C.; Henne, S.; Hoyle, C. R.; Molteni, U.; Herrmann, E.; Adamov, A.; Bukowiecki, N.; et al. New Particle Formation in the Free Troposphere: A Question of Chemistry and Timing. *Science* **2016**, *352*, 1109−1112.

(15) Sindelarova, K.; Granier, C.; Bouarar, I.; Guenther, A.; Tilmes, S.; Stavrakou, T.; Müller, J.-F.; Kuhn, U.; Stefani, P.; Knorr, W. Global Data Set of Biogenic VOC Emissions Calculated by the MEGAN Model over the Last 30 Years. *Atmos. Chem. Phys.* **2014**, *14*, 9317−9341.

(16) Bianchi, F.; Kurtén, T.; Riva, M.; Mohr, C.; Rissanen, M. P.; Roldin, P.; Berndt, T.; Crounse, J. D.; Wennberg, P. O.; Mentel, T. F.; et al. Highly Oxygenated Organic Molecules (HOM) from Gas-Phase Autoxidation Involving Peroxy Radicals: A Key Contributor to Atmospheric Aerosol. *Chem. Rev.* **2019**, *119*, 3472−3509.

(17) Saunders, S. M.; Jenkin, M. E.; Derwent, R. G.; Pilling, M. J. Protocol for the Development of the Master Chemical Mechanism, MCM v3 (Part A): Tropospheric Degradation of Non-Aromatic Volatile Organic Compounds. *Atmos. Chem. Phys.* **2003**, *3*, 161−180.

(18) Park, J.; Jongsma, C. G.; Zhang, R.; North, S. W. OH/OD Initiated Oxidation of Isoprene in the Presence of O_s and NO. *J. Phys. Chem. A.* **2004**, *108*, 10688−10697.

(19) Hoyle, C. R.; Berntsen, T.; Myhre, G.; Isaksen, I. S. A. Secondary Organic Aerosol in the Global Aerosol - Chemical Transport Model Oslo CTM_2. *Atmos. Chem. Phys.* **2007**, *7*, 5675−5694.

(20) Pye, H. O. T.; Chan, A. W. H.; Barkley, M. P.; Seinfeld, J. H. Global Modeling of Organic Aerosol: The Importance of Reactive Nitrogen (NO_x and NO_3). *Atmos. Chem. Phys.* **2010**, *10*, 11261−11276.

(21) Pye, H. O. T.; Luecken, D. J.; Xu, L.; Boyd, C. M.; Ng, N. L.; Baker, K. R.; Ayres, B. R.; Bash, J. O.; Baumann, K.; Carter, W. P. L.; et al. Modeling the Current and Future Roles of Particulate Organic Nitrates in the Southeastern United States. *Environ. Sci. Technol.* **2015**, *49*, 14195−14203.

(22) Huang, M.; Zhang, W.; Gu, X.; Hu, C.; Zhao, W.; Wang, Z.; Fang, L. Size Distribution and Chemical Composition of Secondary Organic Aerosol Formed from Cl-Initiated Oxidation of Toluene. *J. Environ. Sci.* **2012**, *24*, 860−864.

(23) Lee, B. H.; Mohr, C.; Lopez-Hilfiker, F. D.; Lutz, A.; Hallquist, M.; Lee, L.; Romer, P.; Cohen, R. C.; Iyer, S.; Kurtén, T.; et al. Highly Functionalized Organic Nitrates in the Southeast United States: Contribution to Secondary Organic Aerosol and Reactive Nitrogen Budgets. *Proc. Natl. Acad. Sci. U. S. A.* **2016**, *113*, 1516−1521.

(24) Geyer, A.; Alicke, B.; Ackermann, R.; Martinez, M.; Harder, H.; Brune, W.; Di Carlo, P.; Williams, E.; Jobson, T.; Hall, S.; Shetter, R.; Stutz, J. Direct Observations of Daytime NO_3: Implications for Urban Boundary Layer Chemistry. *J. Geophys. Res. Atmos.* **2003**, *108*, 1−11.

(25) Ayres, B. R.; Allen, H. M.; Draper, D. C.; Brown, S. S.; Wild, R. J.; Jimenez, J. L.; Day, D. A.; Campuzano-Jost, P.; Hu, W.; de Gouw, J.; Koss, A. R.; Cohen, R. C.; Duffey, K. C.; Romer, P. S.; Baumann, K.; Edgerton, E. S.; Takahama, S.; Thornton, J. A.; Lee, B. H.; Lopez-Hilfiker, F. D.; Mohr, C.; Goldstein, A. H.; Olson, K.; Fry, J. L. Organic Nitrate Aerosol Formation via NO_3 and BVOC in the Southeastern US. *Atmos. Chem. Phys. Discuss.* **2015**, *15*, 16235−16272.

(26) Rollins, A. W.; Browne, E. C.; Min, K.-E.; Pusede, S. E.; Wooldridge, P. J.; Gentner, D. R.; Goldstein, A. H.; Liu, S.; Day, D. A.; Russell, L. M.; Cohen, R. C. Evidence for NO_x Control over Nighttime SOA Formation. *Science* **2012**, *337*, 1210−1212.

(27) Fry, J. L.; Draper, D. C.; Zarzana, K. J.; Campuzano-Jost, P.; Day, D. A.; Jimenez, J. L.; Brown, S. S.; Cohen, R. C.; Kaser, L.;

Hansel, A.; et al. Observations of Gas- and Aerosol-Phase Organic Nitrates at BEACHON-RoMBAS 2011. *Atmos. Chem. Phys.* **2013**, *13*, 8585−8605.
(28) Kiendler-Scharr, A.; Mensah, A. A.; Friese, E.; Topping, D.; Nemitz, E.; Prevot, A. S. H.; Äijälä, M.; Allan, J.; Canonaco, F.; Canagaratna, M.; et al. Ubiquity of Organic Nitrates from Nighttime Chemistry in the European Submicron Aerosol. *Geophys. Res. Lett.* **2016**, *43*, 7735−7744.
(29) Ng, N. L.; Brown, S. S.; Archibald, A. T.; Atlas, E.; Cohen, R. C.; Crowley, J. N.; Day, D. A.; Donahue, N. M.; Fry, J. L.; Fuchs, H.; et al. Nitrate Radicals and Biogenic Volatile Organic Compounds: Oxidation, Mechanisms, and Organic Aerosol. *Atmos. Chem. Phys.* **2017**, *17*, 2103−2162.
(30) Kubečka, J.; Besel, V.; Kurtén, T.; Myllys, N.; Vehkamäki, H. Configurational Sampling of Noncovalent (Atmospheric) Molecular Clusters: Sulfuric Acid and Guanidine. *J. Phys. Chem. A* **2019**, *123*, 6022−6033.
(31) *Spartan 16*; Wavefunction Inc.: Irvine, C. A., 2016.
(32) Møller, K. H.; Otkjær, R. V.; Hyttinen, N.; Kurtén, T.; Kjaergaard, H. G. Cost-Effective Implementation of Multiconformer Transition State Theory for Peroxy Radical Hydrogen Shift Reactions. *J. Phys. Chem. A* **2016**, *120*, 10072−10087.
(33) Zhang, J.; Dolg, M. Global Optimization of Clusters of Rigid Molecules Using the Artificial Bee Colony Algorithm. *Phys. Chem. Chem. Phys.* **2016**, *18*, 3003−3010.
(34) Zhang, J.; Dolg, M. ABCluster: The Artificial Bee Colony Algorithm for Cluster Global Optimization. *Phys. Chem. Chem. Phys.* **2015**, *17*, 24173−24181.
(35) Glendening, E. D.; Reed, A. E.; Carpenter, J. E.; Weinhold, F. *NBO, Version 3.1.*; Gaussian Inc., 2003.
(36) Grimme, S.; Bannwarth, C.; Shushkov, P. A Robust and Accurate Tight-Binding Quantum Chemical Method for Structures, Vibrational Frequencies, and Noncovalent Interactions of Large Molecular Systems Parametrized for All Spd-Block Elements (Z = 1-86). *J. Chem. Theory Comput.* **2017**, *13*, 1989−2009.
(37) Lee, C.; Yang, W.; Parr, R. G. Development of the Colle-Salvetti Correlation-Energy Formula into a Functional of the Electron Density. *Phys. Rev. B* **1988**, *37*, 785−789.
(38) Hehre, W. J.; Ditchfield, R.; Pople, J. A. Self-Consistent Molecular Orbital Methods. XII. Further Extensions of Gaussian−Type Basis Sets for Use in Molecular Orbital Studies of Organic Molecules. *J. Chem. Phys.* **1977**, *56*, 2257.
(39) Frisch, M. J.; Trucks, G. W.; Schlegel, H. B.; Scuseria, G. E.; Robb, M. A.; Cheeseman, J. R.; Scalmani, G.; Barone, V.; Petersson, G. A.; Nakatsuji, H.; Li, X.; Caricato, M.; Marenich, A.V.; Bloino, J., Janesko, B.G., Gomperts, R., Mennucci, B., Hratchian, H.P., Ortiz, J.V., Izmaylov, A.F., Sonnenberg, J.L., Williams-Young, D., Ding, F., Lipparini, F., Egidi, F., Goings, J., Peng, B., Petrone, A., Henderson, T., Ranasinghe, D., Zakrzewski, V.G., Gao, J., Rega, N., Zheng, G., Liang, W., Hada, M., Ehara, M., Toyota, K., Fukuda, R., Hasegawa, J., Ishida, M., Nakajima, T., Honda, Y., Kitao, O., Nakai, H., Vreven, T., Throssell, K., Montgomery, Jr., J.A., Peralta, J.E., Ogliaro, F., Bearpark, M.J., Heyd, J.J., Brothers, E.N., Kudin, K.N., Staroverov, V.N., Keith, T.A., Kobayashi, R., Normand, J., Raghavachari, K., Rendell, A.P., Burant, J.C., Iyengar, S.S., Tomasi, J., Cossi, M., Millam, J.M., Klene, M., Adamo, C., Cammi, R., Ochterski, J.W., Martin, R.L., Morokuma, K., Farkas, O., Foresman, J.B., Fox, D.J. *Gaussian 16, Revision B.01*; Gaussian, Inc.: Wallingford CT, 2016.
(40) Granovsky, A. A. Firefly version 8.2.0. http://classic.chemss.msu.su/gran/firefly/index.html (accessed November 18, 2021).
(41) Schmidt, M. W.; Baldridge, K. K.; Boatz, J. A.; Elbert, S. T.; Gordon, M. S.; Jensen, J. H.; Koseki, S.; Matsunaga, N.; Nguyen, K. A.; Su, S.; et al. General Atomic and Molecular Electronic Structure System. *J. Comput. Chem.* **1993**, *14*, 1347−1363.
(42) Minaev, B. F.; Ågren, H. The Role of One-Center Spin-Orbit Coupling in Organic Chemical Reactions. *EPA Newsletter* **1999**, *65*, 7−38.
(43) Minaev, B. F.; Lunell, S. Classification of Spin-Orbit Coupling Effects in Organic Chemical Reactions. *Z. Phys. Chem.* **1993**, *182*, 263−284.

https://doi.org/10.1021/acs.jpca.1c08969
J. Phys. Chem. A 2021, 125, 10632−10639